Hindawi
Shock and Vibration
Volume 2021, Article ID 8895583, 19 pages
https://doi.org/10.1155/2021/8895583

Research Article

Mode Shape Description and Model Updating of Axisymmetric Structures Using Radial Tchebichef Moment Descriptors

C. Zang,[1] **H. B. Lan**,[1] **D. D. Jiang**,[2] **and M. I. Friswell**[3]

[1]*Jiangsu Province Key Laboratory of Aerospace Power System, College of Energy and Power Engineering, Nanjing University of Aeronautics and Astronautics, Nanjing 210016, China*
[2]*Shanghai Institute of Space Propulsion, Shanghai 201112, China*
[3]*College of Engineering, Swansea University, SA1 8EN, Swansea, UK*

Correspondence should be addressed to C. Zang; c.zang@nuaa.edu.cn

Received 12 October 2020; Revised 19 January 2021; Accepted 25 February 2021; Published 10 March 2021

Academic Editor: Gilbert R. Gillich

A novel approach for mode shape feature extraction and model updating of axisymmetric structures based on radial Tchebichef moment (RTM) descriptors is proposed in this study. The mode shape features extracted by RTM descriptors can effectively compress the full-field modal vibration data and retain the most important information. The reconstruction of mode shapes using RTM descriptors can accurately describe the mode shapes, and the simulation shows that the RTM function is superior to Zernike moment function in terms of its mathematical properties and its shape reconstruction ability. In addition, the proposed modal correlation coefficient of the RTM amplitude can overcome the main disadvantage of using the modal assurance criterion (MAC), which has difficulty in identifying double or close modes of symmetric structures. Furthermore, the model updating of axisymmetric structures based on RTM descriptors appears to be more efficient and effective than the normal model updating method directly using modal vibration data, avoids manipulating large amounts of mode shape data, and speeds up the convergence of updating parameters. The RTM descriptors used in correlation analysis and model updating are demonstrated with a cover of an aeroengine rig. The frequency deviation between the test and the FE model was reduced from 17.13% to 1.23% for the first 13 modes via the model updating process. It verified the potential to industrial application with the proposed method.

1. Introduction

An accurate and validated finite element (FE) model of a structure is able to predict the dynamic characteristics of structures, such as natural frequencies and mode shapes, with high precision [1, 2]. The modal assurance criterion (MAC) [3], which is defined as the cosine of the angle between the predicted and measured eigenvectors, is the most commonly used method to evaluate discrepancies of mode shapes between the analytical prediction and the measured. This is a valuable tool in mode matching and takes a key step in model updating. However, using only the MAC to represent the correlation of the FE model and the test has a crucial limitation since its value will be affected by the number and location of the comparative points. For large and complex structures, it is difficult to use the MAC to describe variations of mode shapes, either locally or globally. Further difficulties occurred with the development of vibration testing technology such as the laser Doppler vibrometer (LDV) [4, 5], where the full-field vibration mode data can be obtained with a significantly increased number of measured points. One of the main limitations of the MAC for large vibration datasets is that it only reflects the simple comparison between two arrays, which restricts the extraction of features from vibration data and hence reduces the significance of any comparison of these features. Another important limitation is that the MAC struggles to identify double modes in symmetrical structures, where the modes have close frequencies and similar mode shapes, but a rotation angle exists between the mode shapes.

For model updating, the vibration data includes a wealth of information on the vibration characteristics. Hence, by applying model updating using the measured data, the updated model will represent more closely to the actual

structural dynamics. However, the mode shape data are commonly used for correlation analysis and rarely used in updating directly due to the size of the modal data and the lack of sensitivity with respect to the updating parameters.

In recent years, image processing techniques have been introduced into dynamics. Molina-Viedma [6] used high-speed 3D digital image correlation for full-field modal analysis. The concept of the moment function from image processing was put forward by Hu [7] in 1962 who defined the geometric moment in terms of translation, rotation, and scaling invariants. Subsequently, rotational moments [8], regular moments [9], and complex geometric moments [10] were proposed. However, the kernel functions of these moments are not orthogonal, and there were data redundancies when using them to extract image features. Teague [11] proposed Zernike moments that satisfy orthogonality in 1980 and used these Zernike moments to exact shape features from an image, with benefits of properties of orthogonality, rotation invariance, and low noise sensitivity. Teh and Chin [12] compared geometric, Legendre, Zernike, pseudo-Zernike, rotational, and complex moments in image expression ability, noise sensitivity, and information redundancy and showed that overall, the performance of Zernike moments superseded the alternative five moments. Since then, Zernike moments have been widely used in image recognition technology [13], image digital watermarking technology [14], structure modal analysis [15], and so on. However, Zernike polynomials are continuous functions, whereas the image domain is discrete, and so there will be discretization errors that lead to inaccuracies. Thus, Mukundan [16] proposed the discrete orthogonal Tchebichef moments, which overcame the numerical errors introduced by kernel discretization and made the calculation more accurate. Later, other discrete orthogonal moments were also proposed, such as Krawtchouk [17], Racah [18], and Dual Hahn moments [19]. These moments do not account for rotational invariance, which is a major drawback, and so, they are unsuitable for pattern recognition and identification. Mukundanet al. [20] proposed the radial Tchebichef moments, constructed by Tchebichef moments and trigonometric functions. Compared to other moments, the radial Tchebichef moments have many advantages: (1) orthogonal kernel functions support minimal information redundancy when extracting image features, (2) discrete kernel functions prevents the discrete approximation of continuous integrals of the moments, and (3) rotational invariance allows circular structures to be processed.

Given the aforementioned advantages, Wang et al. [21, 22] were the first to successfully apply Tchebichef and Zernike moments in structural dynamics to extract features of the mode shapes. The Zernike moments were used to analyze three different structures: a disk, rectangular plate, and a disk with added mass, where the mode shapes were extracted and used for correlation analysis. The Tchebichef moments were used to extract shape features and perform correlation analysis and model updating for a composite sandwich panel. Zang et al. [23, 24] also conducted research on Zernike and Tchebichef moments and successfully applied Zernike moments to the model updating of an aeroengine disk.

This study introduces a novel radial Tchebichef moment into the field of structural dynamics for model correlation analysis and updating. Section 2 introduces the basic concept and computing method of radial Tchebichef moments to extract features of mode shapes images and the model correlation and updating methods based on the RTMs. The further correlation analysis of a simulated disk using RTMs is introduced in Section 3. Model updating based on RTMs is demonstrated with a practical structure of an aeroengine test rig cover in Section 4. Finally, the conclusion is discussed in Section 5.

2. Shape Descriptors for Correlation and Model Updating

2.1. Radial Tchebichef Moment Descriptors. For an image of size $N \times N$, the radial Tchebichef moment descriptors of order p with repetition q for a given mode shape $\psi(r, \vartheta)$ expressed in polar coordinates is defined as [25]

$$R_{pq} = \frac{1}{\rho(p, (N/2))} \sum_{r=0}^{(N/2)-1} t_p(r) \sum_{k=0}^{m-1} \frac{1}{m} e^{-jq\vartheta} \psi(r, \vartheta), \quad (1)$$

where $\vartheta = (2\pi qk/m)$, and $t_p(r)$ is the p^{th} Tchebichef polynomial, defined as

$$t_p(r) = \frac{p!}{(N/2)^p} \sum_{k=0}^{p} (-1)^{p-k} \binom{\binom{N}{2} - 1 - k}{p-k} \binom{p+k}{p} \binom{r}{k}. \quad (2)$$

In equation (1), $\rho(p, (N/2))$ is defined as

$$\rho\left(p, \left(\frac{N}{2}\right)\right) = \sum_{r=0}^{(N/2)-1} \left\{t_p(r)\right\}^2. \quad (3)$$

According to equation (1), the radial Tchebichef moment descriptors can be extracted from a mode shape image, and the radial Tchebichef moments is represented as a vector: $\mathbf{R}^{\mathrm{T}} = \left\{R_{00}, R_{01}, R_{02}, \ldots, R_{10}, R_{11}, R_{12}, \ldots, R_{p,q}\right\}$, where $p = 0, 1, 2, \ldots, (N/2) - 1; q = 0, 1, 2, \ldots, m$.

The radial Tchebichef moments R_{pq} in equation (1) are complex numbers. If we use $R_{pq}^{(\mathrm{re})}$ to represent the real part and $R_{pq}^{(\mathrm{im})}$ to represent the imaginary part of R_{pq}, then $R_{pq}^{(\mathrm{re})}$ and $R_{pq}^{(\mathrm{im})}$ can be expressed as

$$R_{pq}^{(\mathrm{re})} = C_{pq} = \frac{1}{\rho(p, (N/2))} \sum_{r=0}^{(N/2)-1} t_p(r) \sum_{k=0}^{m-1} \frac{1}{m} \cos\, q\vartheta \psi(r, \vartheta), \quad (4)$$

$$R_{pq}^{(\mathrm{im})} = S_{pq} = \frac{1}{\rho(p, (N/2))} \sum_{r=0}^{(N/2)-1} t_p(r) \sum_{k=0}^{m-1} \frac{1}{m} \sin\, q\vartheta \psi(r, \vartheta). \quad (5)$$

Assuming that the mode shape image rotates at an angle α around the image center, the rotated mode shape becomes another image $\psi'(r, \vartheta)$, where relationship between $\psi(r, \vartheta)$ and $\psi'(r, \vartheta)$ may be expressed as

$$\psi'(r,\vartheta) = \psi(r,\vartheta-\alpha). \tag{6}$$

Hence, the relation between radial Tchebichef moments $\psi'(r,\vartheta)$ and $\psi(r,\vartheta)$ is expressed as

$$R_{pq}{}' = R_{pq}e^{-\mathrm{jq}\alpha}. \tag{7}$$

Equation (7) indicates that the rotated image has the same amplitude of the radial Tchebichef moment as the original image, that is,$|R_{pq}{}'| = |R_{pq}|$, and so, the amplitude of the radial Tchebichef moment is rotational invariant. In addition, the phase of the RTM can be used to compute the rotational angle of double modes expressed as

$$\alpha = \frac{\arg\left(R_{pq}\right) - \arg\left(R_{pq}{}'\right)}{q}. \tag{8}$$

Equation (8) is an important property for the use of RTM descriptors in modal analysis of double modes.

Since the RTMs have been calculated, the original image can be reconstructed with a truncated expansion of the RTMs as

$$\begin{aligned}\psi(r,\vartheta) \cong & \sum_{p=0}^{p\max} t_p(r)R_{p0}^{(\mathrm{re})} \\ & + 2\sum_{q=1}^{(m/2)}\left(\sum_{p=0}^{p\max} t_p(r)R_{pq}^{(\mathrm{re})}\cos q\vartheta + \sum_{p=0}^{p\max} t_p(r)R_{pq}^{(\mathrm{im})}\sin q\vartheta\right),\end{aligned} \tag{9}$$

where $p_{\max}$ denotes the maximum order of the reconstructed moments, and R_{pq}^{re} and R_{pq}^{im} are given by equation (4) and equation (5), respectively.

2.2. Correlation Analysis. The modal assurance criterion (MAC) descriptor, also called the modal correlation coefficient, is the most common correlation method in modal analysis. The MAC is defined as

$$\mathbf{MAC}(i,j) = \frac{\left|\left\{\phi_i^e\right\}^T\left\{\phi_j^a\right\}\right|^2}{\left(\left\{\phi_i^e\right\}^T\left\{\phi_i^e\right\}\right)\left(\left\{\phi_j^a\right\}^T\left\{\phi_j^a\right\}\right)}. \tag{10}$$

where the superscript T represents the matrix transpose, $\{\phi_i^e\}$is the i^{th} mode shape from the test, and $\{\phi_j^a\}$ is the j^{th} mode shape from the FE model.

Following a similar definition to the MAC, the correlation coefficient of the radial Tchebichef moment amplitude is defined as

$$\mathbf{R}_{\mathrm{mac}}(i,j) = \frac{\left|\left\{\mathbf{R}_i^e\right\}^H\left\{\mathbf{R}_j^a\right\}\right|^2}{\left(\left\{\mathbf{R}_i^e\right\}^H\left\{\mathbf{R}_i^e\right\}\right)\left(\left\{\mathbf{R}_j^a\right\}^H\left\{\mathbf{R}_j^a\right\}\right)}, \tag{11}$$

where H represents the conjugate transpose, and $\{\mathbf{R}_i^e\}$ and $\{\mathbf{R}_j^a\}$denote the vector of the i^{th} radial Tchebichef moment of the test data and the vector of the j^{th} radial Tchebichef moment of the FE model data, respectively.

The values of the MAC and the correlation coefficient for the RTMs are within the range from zero to one. The closer is the coefficient to one, the higher the correlation of the two modes. If the value is zero, the two modes are uncorrelated. The two models in the correlation analysis can be from various model combinations, such as FEM/test, FEM/FEM, or both from tests (test/test). From the definition of the MAC, its value reflects a simple comparison of two vectors in a discrete space. However, the correlation analysis using RTMs contains the main information of the mode shape and the rotational invariance, meaning that it is not affected by rotation of the mode shape.

2.3. Model Updating Based on RTMs. In the rectangular coordinate system, equation (1) can be expressed as

$$\begin{aligned}R_{pq} &= \frac{1}{\rho(p,(N/2))}\sum_{r=0}^{(N/2)-1} t_p(r)\sum_{k=0}^{m-1}\frac{1}{m}e^{-jq\vartheta}\psi(r,\vartheta) \\ &= \sum_{x=0}^{N-1}\sum_{y=0}^{N-1} V_{pq}(x,y)\psi(x,y,\theta),\end{aligned} \tag{12}$$

where θ is an updating parameter. The sensitivity of the RTM with respect to θ can be written as

$$\begin{aligned}S_{R_{pq}} &= \frac{\partial R_{pq}}{\partial\theta} = \frac{\partial\left[\sum_{x=0}^{N-1}\sum_{y=0}^{N-1}V_{pq}(x,y)\psi(x,y,\theta)\right]}{\partial\theta} \\ &= \sum_{x=0}^{N-1}\sum_{y=0}^{N-1} V_{pq}(x,y)\frac{\partial\psi(x,y,\theta)}{\partial\theta}.\end{aligned} \tag{13}$$

For general vibration problems, the vibration displacement of the structure $w(x,y,t)$ can be represented by the Rayleigh Ritz method as

$$\mathbf{w}(x,y,\theta) = \sum_i^n \pi_i(x,y)q_i(t), \tag{14}$$

where the variable $\pi_i(x,y)$ is the i^{th} shape function and only depends on the structural coordinates x and y, and n is the number of degrees of freedom. If a single modal response is excited, then $q_i(t)$ can be expressed as

$$\{q_i\} = \{\phi_i\}\sin\,\omega t, \tag{15}$$

where $\{\phi_i\}$ is the eigenvector. The vibration displacement is rewritten by substituting equation (15) into equation (14) to give

$$\mathbf{w}(x,y,\theta) = \boldsymbol{\pi}^T(x,y)\phi(\theta)\sin\,\omega t. \tag{16}$$

Therefore, the continuous mode shape $\psi(x,y,\theta)$ can be expressed as a linear combination of the discrete eigenvectors $\phi(\theta)$ and $\pi^T(x,y)$, which is a matrix of prescribed linear-independent trial functions in terms of x and y. Thus,

$$\psi(x,y,\theta) = \pi^{\mathrm{T}}(x,y)\phi(\theta). \tag{17}$$

Substituting equation (20) into equation (13) gives

$$S_R = \frac{\partial\left[\sum_{x=0}^{N-1}\sum_{y=0}^{N-1} V_{pq}(x,y)\pi^{\mathrm{T}}(x,y)\phi(\theta)\right]}{\partial\theta} = \sum_{x=0}^{N-1}\sum_{y=0}^{N-1} V_{pq}(x,y)\pi^{T}(x,y)\frac{\partial\phi(\theta)}{\partial\theta}. \quad (18)$$

Equation (21) indicates that the sensitivity of RTM with respect to the updating parameter θ can be obtained by RTMs of $\pi(x, y)$ and the sensitivity of the discrete eigenvector with respect to the updating parameterθ.

Without considering the weight matrix, the improved parameter estimate is given as

$$\delta\theta = \left[S_{R,j}^{\mathrm{T}} S_{R,j}\right]^{-1} S_{R,j}^{T}\delta R. \quad (19)$$

So that the updated parameter can be expressed as

$$\theta_{j+1} = \theta_j + \left[S_{R,j}^{\mathrm{T}} S_{R,j}\right]^{-1} S_{R,j}^{T}\left(R_m - R_j\right), \quad (20)$$

where θ_j and θ_{j+1} represent the updating parameters of the current and subsequent steps, $S_{R,j}$ is the current sensitivity matrix, R_m is the result of test, and R_j is the current computed result.

3. Case Study I: Correlation Analysis of a Simulated Disk Using RTMs

3.1. Finite Element Model of the Disk. In this section, a symmetrical structure of the disk, with diameter 200 mm and thickness 4 mm, is used for simulation analysis based on the RTMs to extract features of mode shapes and reconstruction of mode shapes with selected RTMs. A finite element model of the disk is built in PATRAN and shown in Figure 1. The disk is divided into 2521 four-node quadrilateral plate elements, and the boundary conditions are set to free-free. The material properties of the disk are given in Table 1.

The natural frequencies of the first 16 modes were calculated and are listed in Table 2. Figure 2 shows the corresponding mode shapes. From Table 2 and Figure 2, both clearly show several double modes in this perfectly symmetrical structure, giving mode pairs (1, 2), (4, 5), (6, 7), (8, 9), (10, 11), (12, 13), and (15, 16).

From these mode shapes, the z-axis can be identified as the main vibration direction. Hence, mapping the contours of vibration amplitude in the z-direction to colors gives the images as shown in Figure 3. Considering computational efficiency and the requirements of the mode shape reconstruction, the mode shapes are reconstructed using radial Tchebichef moments up to order 15 ($p = 15$), and the results are shown in Figure 4. Comparing Figure 4 with Figure 3, it indicates that an accurate reconstruction of mode shapes can be obtained using the first 15 orders of RTMs.

In order to show the advantage of mode shape reconstruction using radial Tchebichef moments, the Zernike polynomials used in reference [14] are considered here to reconstruct the mode shapes of the disk. The reconstructed

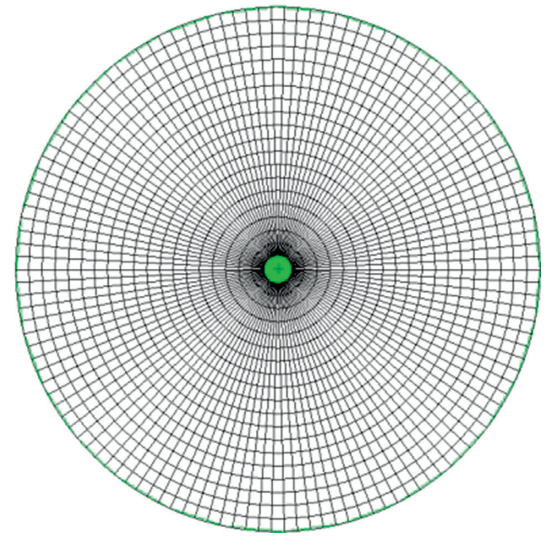

Figure 1: Finite element mesh of the disk.

Table 1: Material properties of the disk.

Mass density	Poisson's ratio	Elasticity modulus
7850 kg/m^3	0.24	199 Gpa

Table 2: Natural frequencies of the finite element model of the disk.

Mode	Natural frequencies (Hz)	Mode	Natural frequencies (Hz)
1	131.72	9	530.46
2	131.72	10	810.15
3	210.49	11	810.15
4	303.75	12	833.36
5	303.75	13	833.36
6	483.47	14	903.91
7	483.47	15	1141.41
8	530.46	16	1141.41

mode shapes using radial Tchebichef moments and Zernike Moments (ZMs), respectively, with different orders ($p = 5$, 10, 20, 40) are compared and plotted in Figure 5. It can be seen that using RTMs to reconstruct mode shapes has obvious advantages. With only a low order of RTMs ($p = 5$), the mode shape images can be reconstructed with a good quality. With the increase of the moment order p, the quality of reconstruction gradually increases not only for the low vibration modes but also for the higher modes with more complex shapes. The radial Tchebichef moment functions are shown to have high stability in image reconstruction. On the contrary, the reconstructed mode shape images using first 5 orders of Zernike moment functions in the initial stage show a relatively good match with the originals, except for modes 15 and 16. The reconstructed shapes reach the best match with the original shapes for all considered modes when the order of ZMs is taken as 10. Afterwards, the reconstructed images for all mode shapes become worse with the increase of the order, and they reach the poorest when the order of ZMs equals 40. Thus, the reconstruction effect using Zernike moment functions is unstable and very

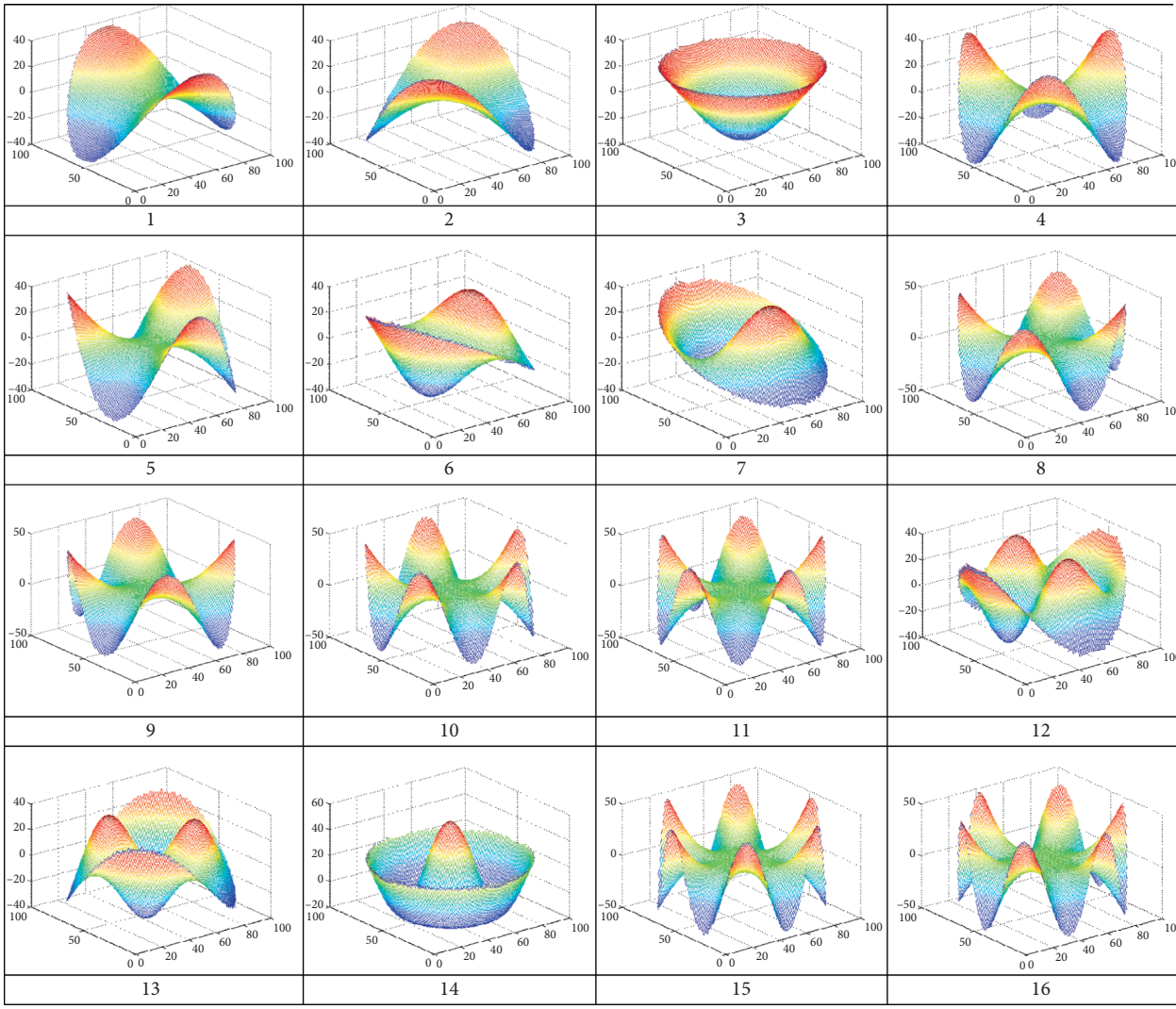

Figure 2: The first 16 vibration mode shapes of the disk.

poor for the more complex mode shapes considered. The radial Tchebichef moment function is superior to Zernike moment function in terms of its mathematical properties and its shape reconstruction ability.

3.2. Correlation Analysis Using RTMs. Correlation analysis is an important tool for model matching, and the MAC is a conventional and most commonly used method. Figure 6 shows the result of autocorrelation or the AutoMAC, where the FE modes are correlated with themselves. The MAC values along the diagonal are close to 1, and the off-diagonal terms are close to zero. However, each of the pair of a double mode has distinct mode shapes, and hence, the MAC values between them are very close to zero. In fact, the shapes of the double modes are very similar to each other, and the difference is only due to small rotations with respect to z-axis, for example, a 45° rotation between modes 1 and 2 and a 30° rotation between modes 4 and 5.

The RTM descriptors can overcome the disadvantage of the MAC in the autocorrelation analysis because of the rotation invariance of the radial Tchebichef moment. Figure 7 shows the correlation coefficients using the radial Tchebichef moment amplitudes. The superiority of the correlation analysis by RTMs is obvious after comparing with the MAC analysis, and the presence of the double modes is clearly visibly as shown in Figure 7. Furthermore, the angle between double modes can be calculated by RTMs. Figure 8 shows the maximum RTM in polar coordinates. Taking modes 4 and 5 as an example, the maximum RTM of the two modes is R_{13}, meaning the repetition is 3 and the angle of the maximum RTM is 90°. The angle between the two modes can be computed by equation (8), and hence,

$$\alpha = \frac{\arg\left(R_{13}\right) - \arg\left(R_{13}'\right)}{3} = \frac{90^{\circ}}{3} = 30^{\circ}. \tag{21}$$

Using the same method, the angles of all of the double modes are given in Table 3.

In Table 3, only the maximum RTM is used to compute rotation angles. However, different principal RTMs can also be used. Table 4 shows that by using the maximum RTM, the

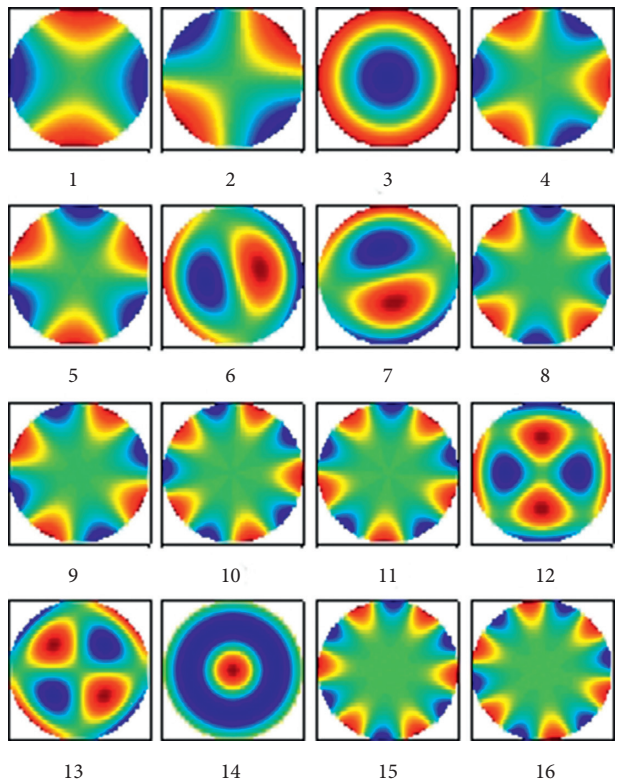

Figure 3: Mode shape contour maps from the FE model.

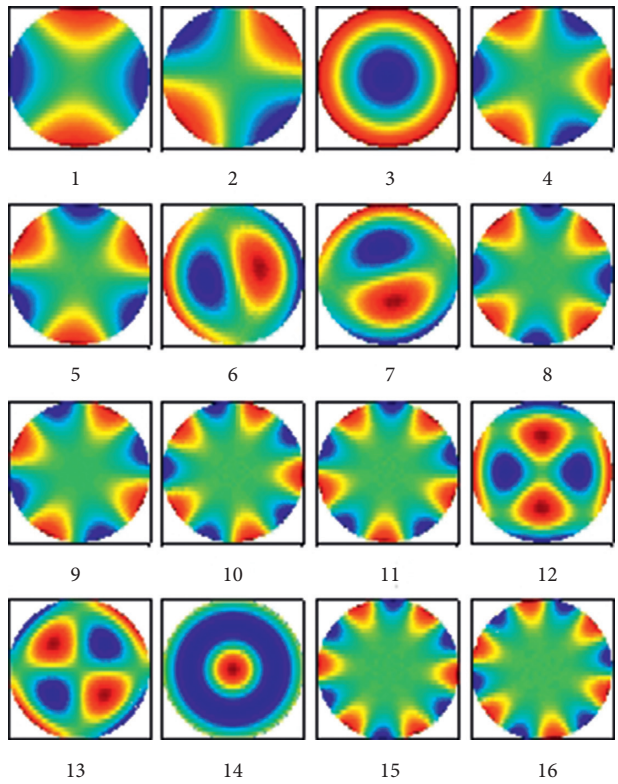

Figure 4: The reconstructed mode shapes of the disk with $p = 15$.

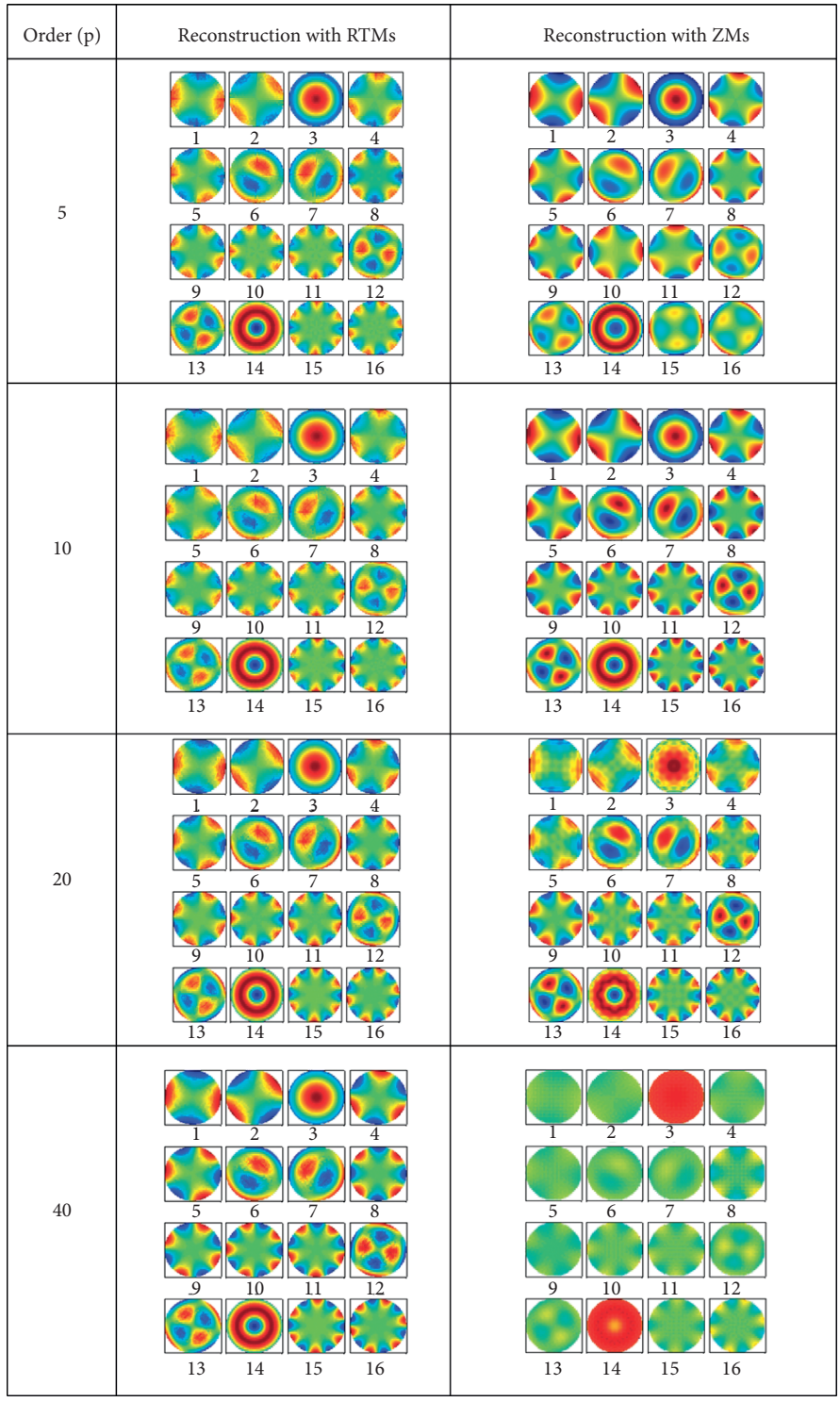

Figure 5: Comparison of the reconstruction of disc mode shapes for different orders.

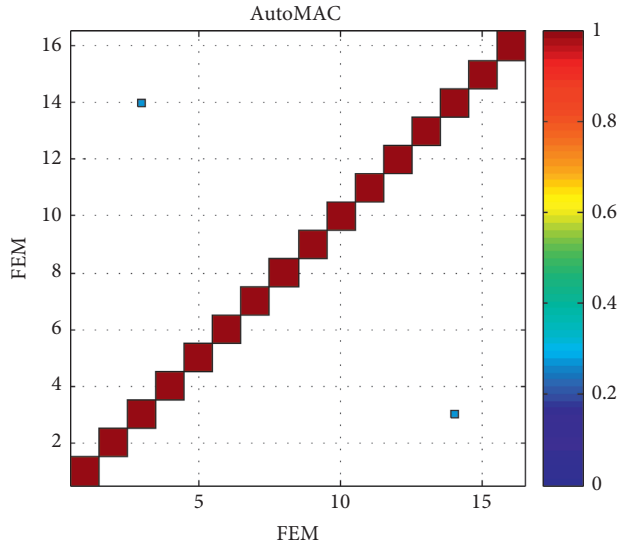

Figure 6: AutoMAC.

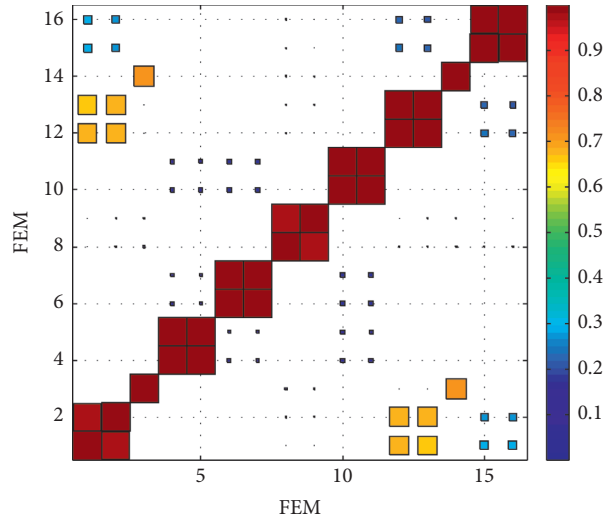

Figure 7: Autocorrelation analysis by RTMs.

2nd RTM and the 3nd RTM to compute rotation angles, consistency can be achieved, thus demonstrating the appropriateness of this method.

4. Case 2: Model Updating Using RTMs

Model updating based on RTMs is now demonstrated on the cover of an aeroengine test rig. A finite element model was developed, a modal test was performed, RTMs were used for correlation, and the model was updated.

4.1. The Modal Test and FE Model of an Aeroengine Test Rig Cover. Figure 9 illustrates the physical shell structure used for this example. Figure 10 shows the FE model in PATRAN, divided into 11093 Tet10 elements, where the boundary conditions are free-free. The material properties of the cover are given in Table 5. The natural frequencies predicted by the FE model of the cover are given in Table 6. As the main vibrations of the cover are in the body, the measuring points are laid on its surface as shown in Figure 11. Figure 12 shows the test model with 49 measurement points. The cover was supported by a compliant sponge mat to simulate the free-free condition, and hammer excitation was used. The natural frequencies of the first 13 modes obtained from the test are shown in Table 7.

Figure 13 shows the vibration mode shape predicted by the FE model, and Figure 14 shows the mode shapes measured by the test. As the main vibration direction is the x-axis (defined in Figure 10), the vibration amplitude of x-axis can be used to specify color contours levels. These contour plots for the FE model and the test are shown in Figures 15 and 16, respectively. The natural frequency predictions show a large difference to the experiments, particularly for modes 6–9.

The RTMs are extracted, and for the first eight modes, the RTM amplitudes are shown in Figures 17 and 18. The results show that only a minority of 500 RTMs are

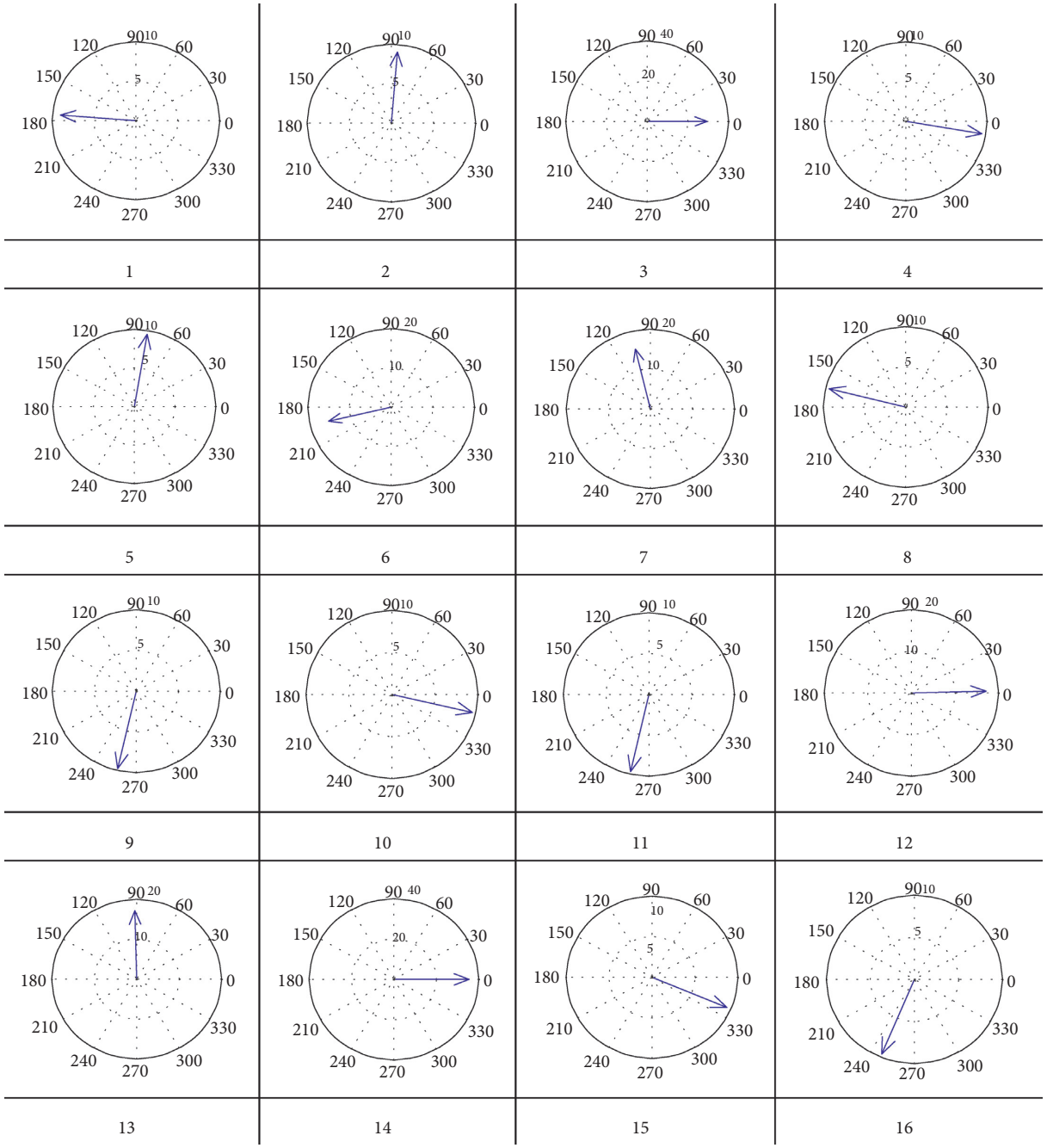

Figure 8: Maximum RTMs.

Table 3: Angles between the double modes.

Double modes	Maximum RTM	Maximum RTM angle	Maximum RTM repetition	Angle of double modes
(1, 2)	R12	89.94	2	44.97
(4, 5)	R13	−90.00	3	−30.00
(6, 7)	R21	89.99	1	89.99
(8, 9)	R14	−90.65	4	−22.66
(10, 11)	R15	89.99	5	18.00
(12, 13)	R22	−89.94	2	−44.97
(15, 16)	R16	89.49	6	14.91

Table 4: Rotation angles using different RTMs.

Double modes	The maximal RTM	The 2nd RTM	The 3rd RTM
(1, 2)	44.97	45.00	45.27
(4, 5)	−30.00	−30.00	−29.99
(6, 7)	89.99	89.98	90.00
(8, 9)	−22.66	−23.17	−20.60
(10, 11)	18.00	17.99	18.03
(12, 13)	−44.97	−45.01	−45.16
(15, 16)	14.91	14.74	16.02

Figure 9: Cover structure.

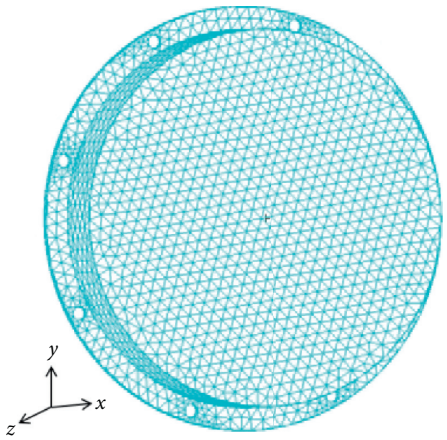

Figure 10: FE mesh of the cover.

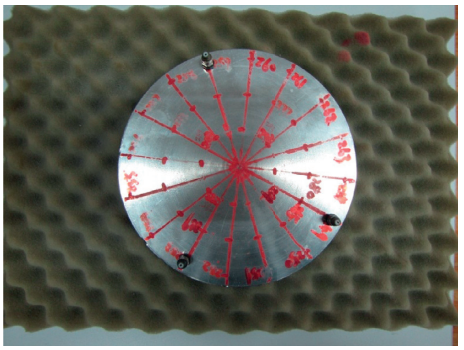

Figure 11: Test configuration of the cover.

Table 5: Material properties of the aeroengine test rig cover.

Density	Poisson's ratio	Elasticity modulus
7900 kg/m^3	0.24	184 GPa

Table 6: Natural frequencies predicted by the FE model of the cover.

Mode	Natural frequency (Hz)	Mode	Natural frequency (Hz)
1	714.40	9	2258.94
2	714.66	10	2780.27
3	787.41	11	3265.81
4	1471.24	12	3266.38
5	1473.49	13	4065.59
6	2251.54	14	4074.88
7	2253.15	15	4299.76
8	2258.86	16	4325.20

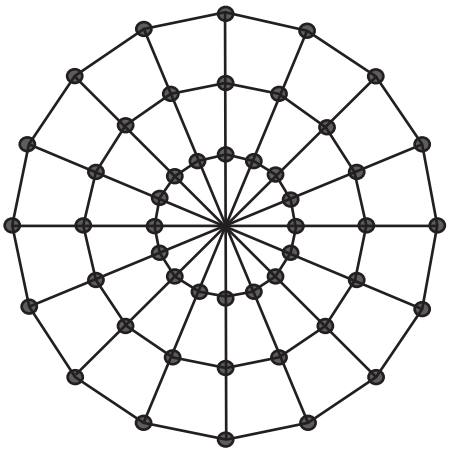

Figure 12: Test model of the cover.

Table 7: Natural frequencies of cover obtained from the experiment.

Mode	Natural frequency (Hz)	Mode	Natural frequency (Hz)
1	634.67	8	2452.27
2	642.16	9	2464.95
3	864.28	10	3019.31
4	1617.86	11	3521.61
5	1620.11	12	3526.16
6	1928.52	13	3912.75
7	1953.65		

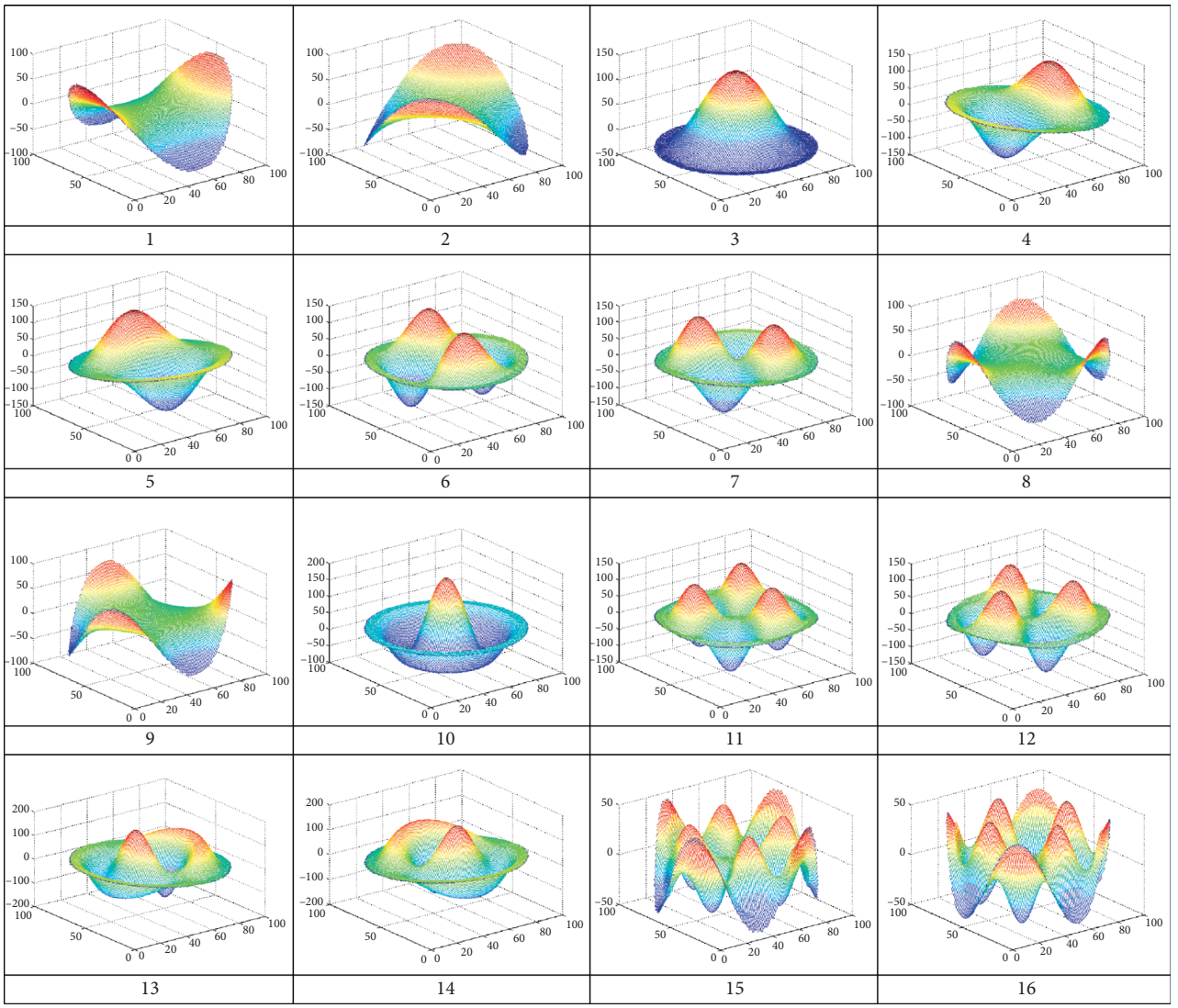

Figure 13: Vibration mode shape predictions from the FE model of the cover.

significant. For each mode, using just a small number of RTMs, the mode shape can be described with precision, and hence, the data are compressed. In addition, there are many RTMs whose amplitudes are smaller in the test than in the prediction and have little effect on the whole shape because the modal test is influenced by noise. Some researchers have shown that choosing suitable RTMs to reconstruct the vibration mode shapes can reduce the influence of noise.

4.2. Correlation Analysis. To analyze the correlation between the prediction and the test, the MAC-based and RTM-based correlation were computed and compared. Figures 19(a) and 19(b) show the autocorrelation of the prediction of the FE model using the MAC and RTM, respectively. Similarly, Figures 20(a) and 20(b) show the autocorrelation of the test using the MAC and RTM, respectively. For the AutoMAC, the value on the diagonal is 1, whereas the other values are closer to zero, meaning the degrees of freedom of this cover

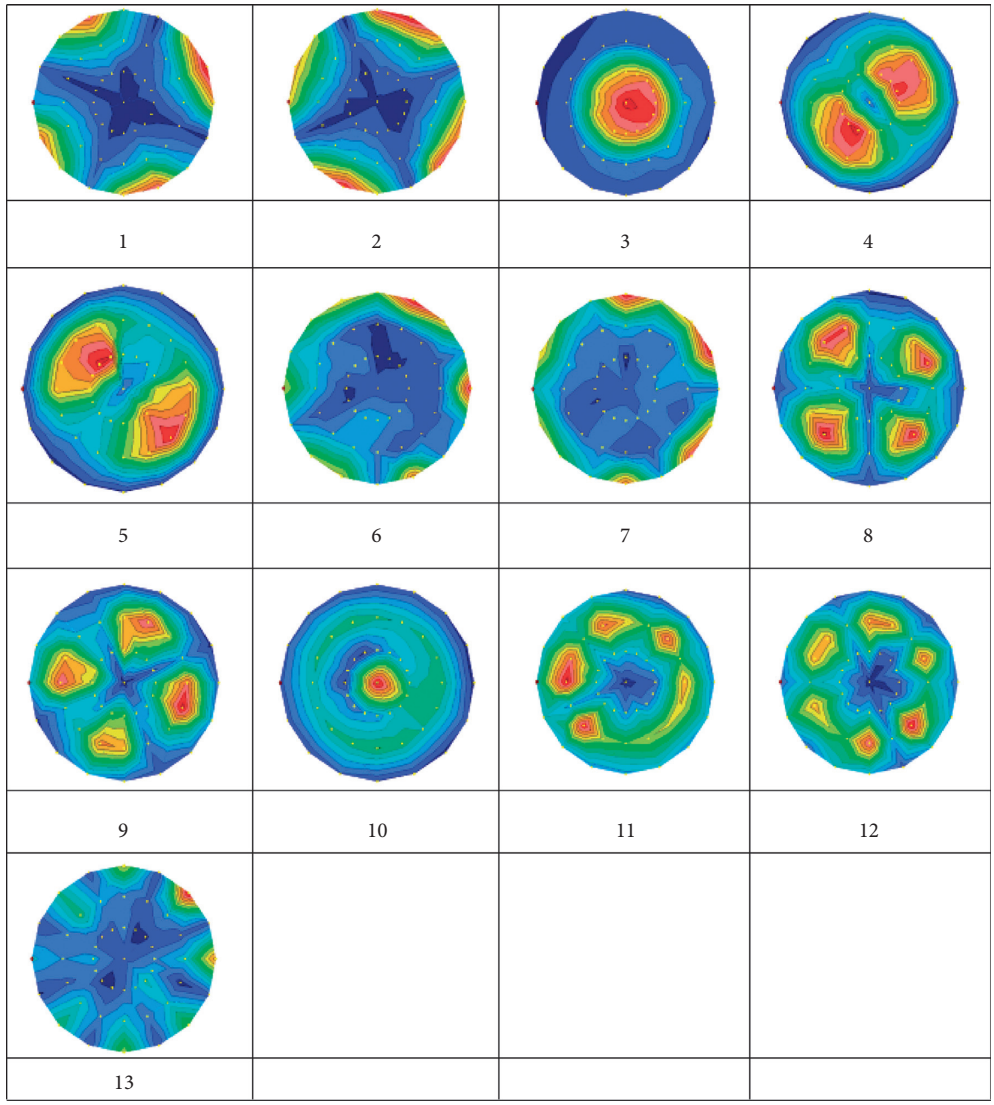

Figure 14: Vibration mode shapes from the test.

structure can be confidently replicated. Figures 19(b) and 20(b) show that the mode shapes with similar characteristics due to double modes are clearly visible using the method based on RTMs.

Figures 21(a) and Figure 21(b) show the correlation between the prediction of the FE model and the test data using the MAC and RTM, respectively. There are now larger values in the off-diagonal terms because of the mismatch between the model and the physical structure. Table 8 shows the detailed numerical results of the correlation analysis, indicating a large frequency deviation between the FE model and the test, with a maximum of 17.13% and a minimum of −7.25%. Due to the interaction of double modes, the highest values of the MAC are smaller than those for the RTMs, which has rotation invariance to overcome the effect of rotational angles in the correlation analysis. For instance, the correlation coefficient values of the RTMs of modes 1 and 2 are significantly larger than those of the MAC.

4.3. Model Updating. Model updating is often necessary because of the differences between the test results and the prediction. After comparing the results of the prediction and the test further, two main causes of the discrepancies can be identified: (i) discretisation errors introduced by finite element modeling and (ii) structure deviation in manufacturing. Figures 22 and 23 show the magnified images of the cover and the FE model. The location of the hole on the side of the cover is significantly different from the location in the design. This problem is compounded by the fact that all of the other holes also have the same error. To resolve this error in the modeling, the FE model of the shell is divided into 4 groups (red, green, blue, and yellow) as shown in Figure 24.

The elastic modulus of the four groups of the material was chosen as the updating parameters, along with the reference data given by the natural frequencies and RTMs from the test. Figure 25 shows the change in frequency deviation and updating parameters over various iterations.

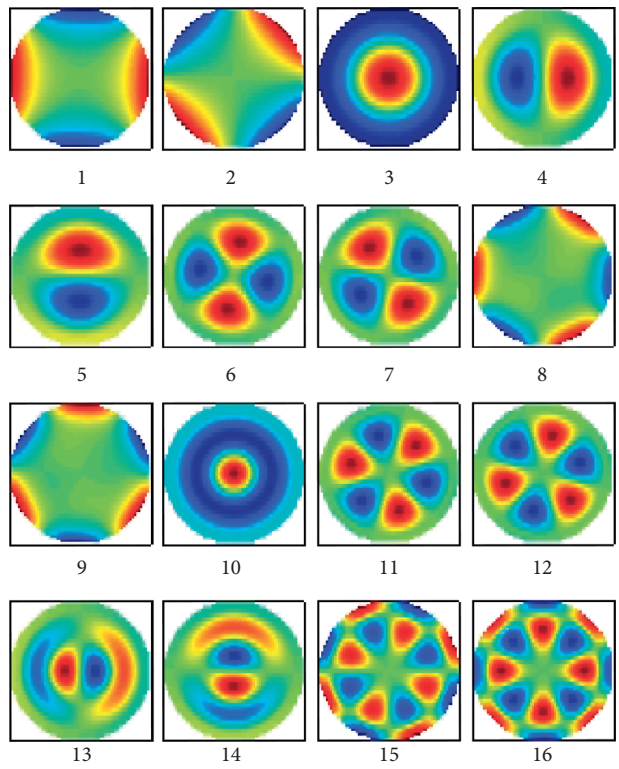

Figure 15: Contour plots of the mode shapes from the FE model of the cover.

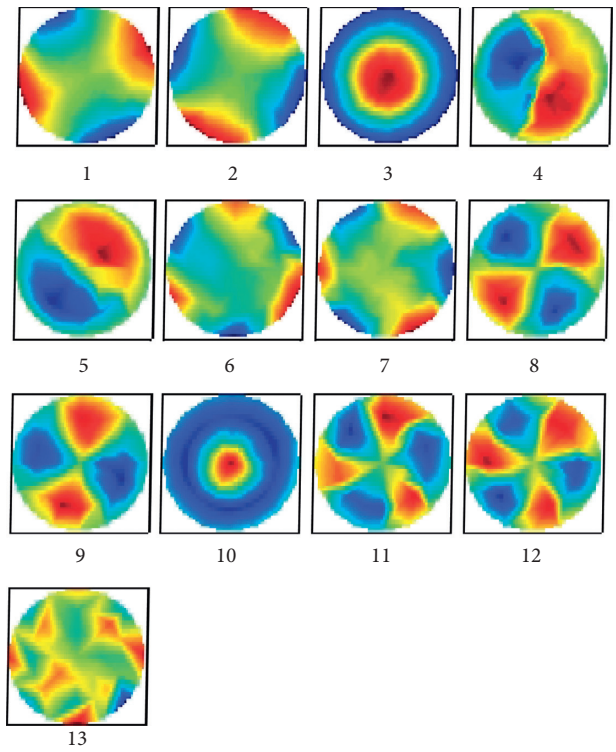

Figure 16: Contour plots of the mode shapes from the test.

After 18 iterations, the updating process converges. Figure 26 shows that the correlation analysis of the FE model after model updating matches the result of the test modes using RTMs. Table 9 shows the comparison of the frequency, MAC, and RT_{MAC} before and after model updating. The data show that after model updating, the frequency deviation is

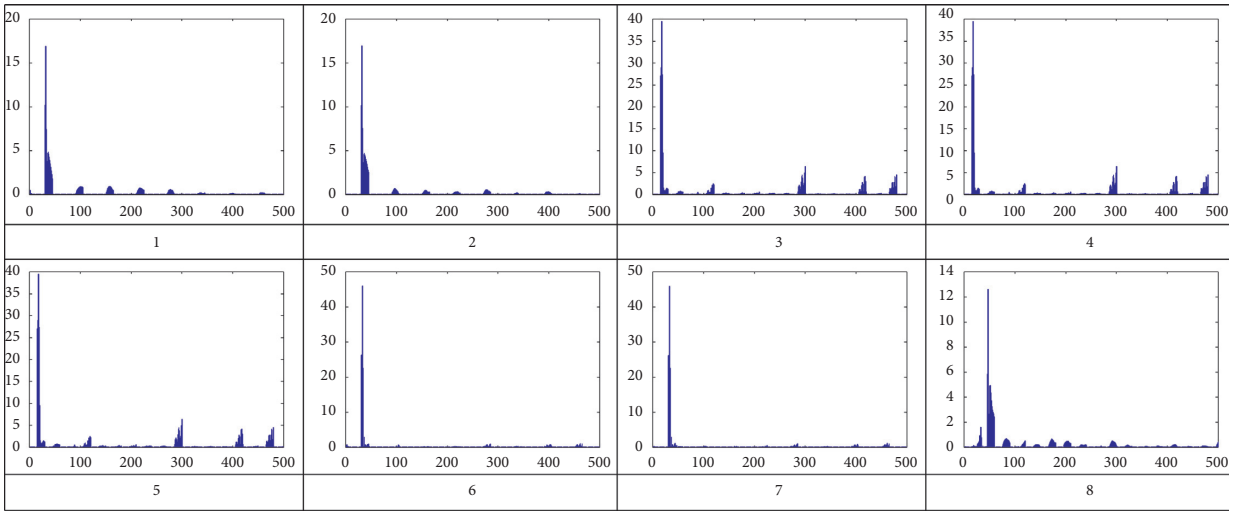

Figure 17: RTMs of the first 8 modes of the FE model.

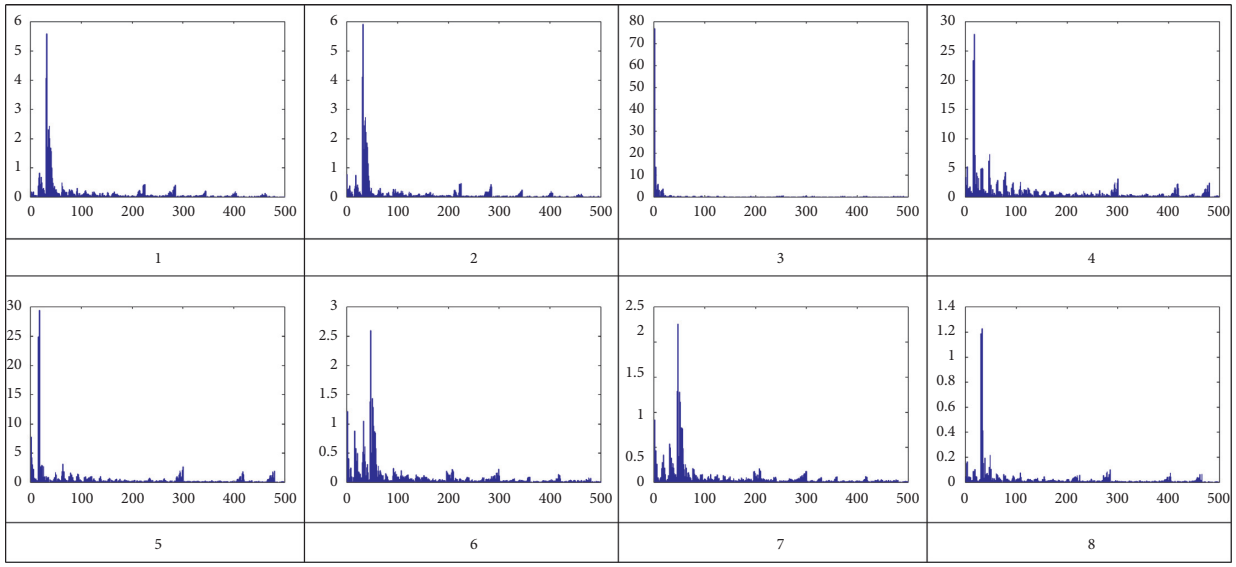

Figure 18: RTMs of the first 8 modes of the test.

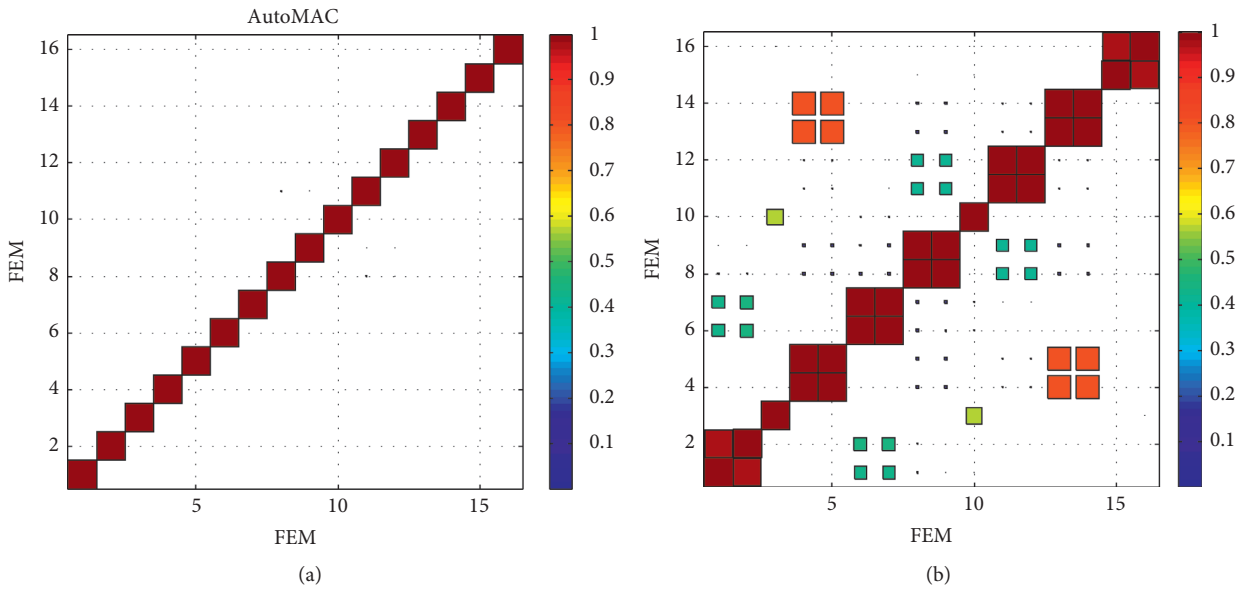

Figure 19: Autocorrelation of the FE model. (a) AutoMAC of the FE model. (b) Autocorrelation analysis by RTMs of the FE model.

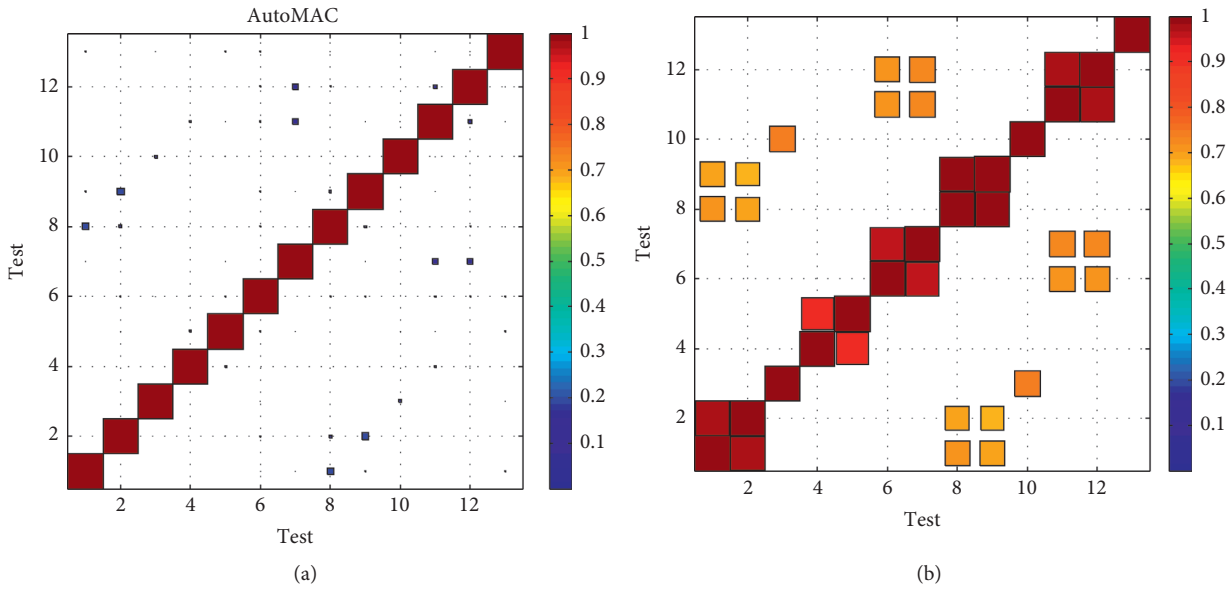

Figure 20: Autocorrelation based on the test data. (a) AutoMAC of the test. (b) Autocorrelation analysis by RTMs of the test.

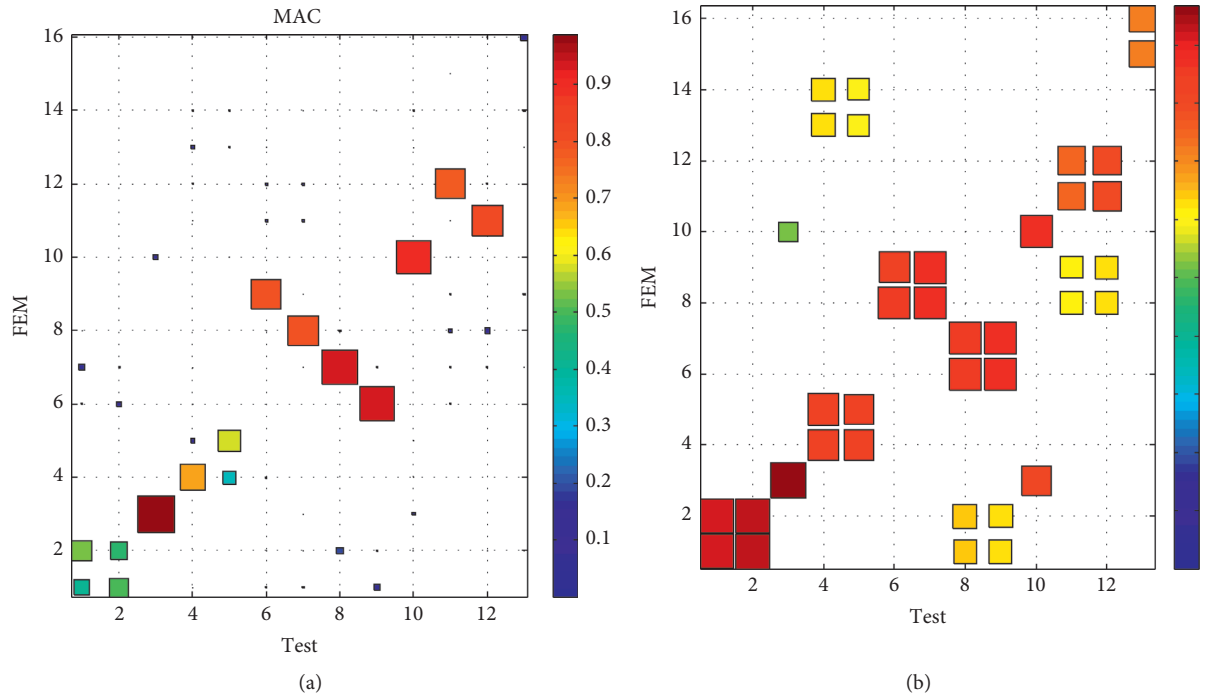

Figure 21: Correlation between the FE model and test. (a) MAC values between the FE model and test. (b) Correlation analysis by RTMs between the FE model and test.

significantly reduced, and the maximum has decreased to 1.23%. Furthermore, the majority of the frequency deviations are smaller than 1%. There is a small increase in the MAC values of the lower modes because the model updating used the RTM data as reference and did not consider the MAC.

After model updating, the changes in the updating parameters are shown in Table 10, where E1–E4 represent the elastic modulus of material groups 1–4. After updating, there was a substantial change in E1 and E3, indicating that the model errors from the holes had significantly influenced these two groups. The changes in E2 and E4 are smaller, and

Table 8: Correlation coefficient and frequency deviation between the FE model and test.

Test		FE model		Frequency deviation (%)	MAC (%)	RT_{MAC} (%)
Mode	Natural frequency (Hz)	Mode	Natural frequency (Hz)			
1	634.67	2	714.66	12.60	53.57	91.74
2	642.16	1	714.40	11.25	49.73	91.74
3	864.28	3	787.41	−8.89	98.78	96.81
4	1617.86	4	1471.24	−9.06	68.15	83.74
5	1620.11	5	1473.49	−9.05	57.89	81.92
6	1928.52	9	2258.94	17.13	78.73	84.68
7	1953.65	8	2258.86	15.62	79.88	86.85
8	2452.27	7	2253.15	−8.12	93.83	86.02
9	2464.95	6	2251.54	−8.66	93.00	86.99
10	3019.31	10	2780.27	−7.92	89.98	87.02
11	3521.61	12	3266.38	−7.25	77.84	75.46
12	3526.16	11	3265.81	−7.38	80.84	79.19
13	3912.75	16	4325.20	10.54	16.45	72.05

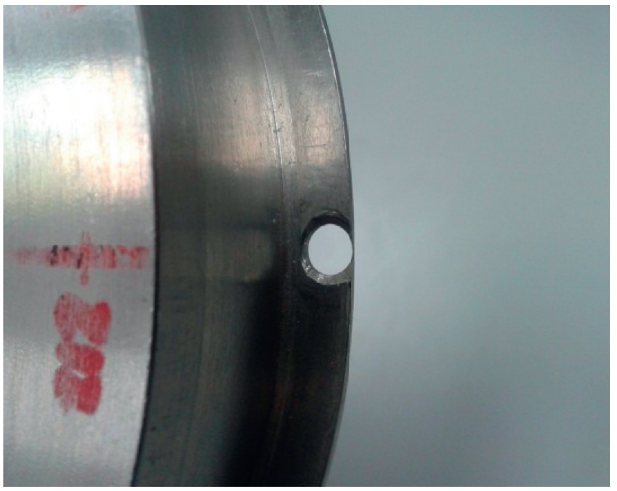

Figure 22: Zoomed image of the flange of the cover.

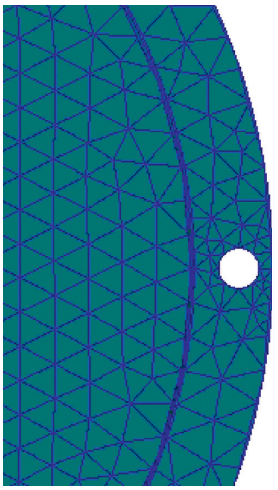

Figure 23: Zoomed image of the FE model.

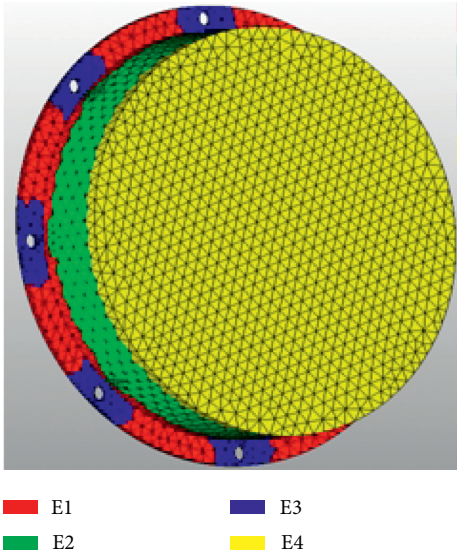

Figure 24: Groups of updating areas of the cover structure.

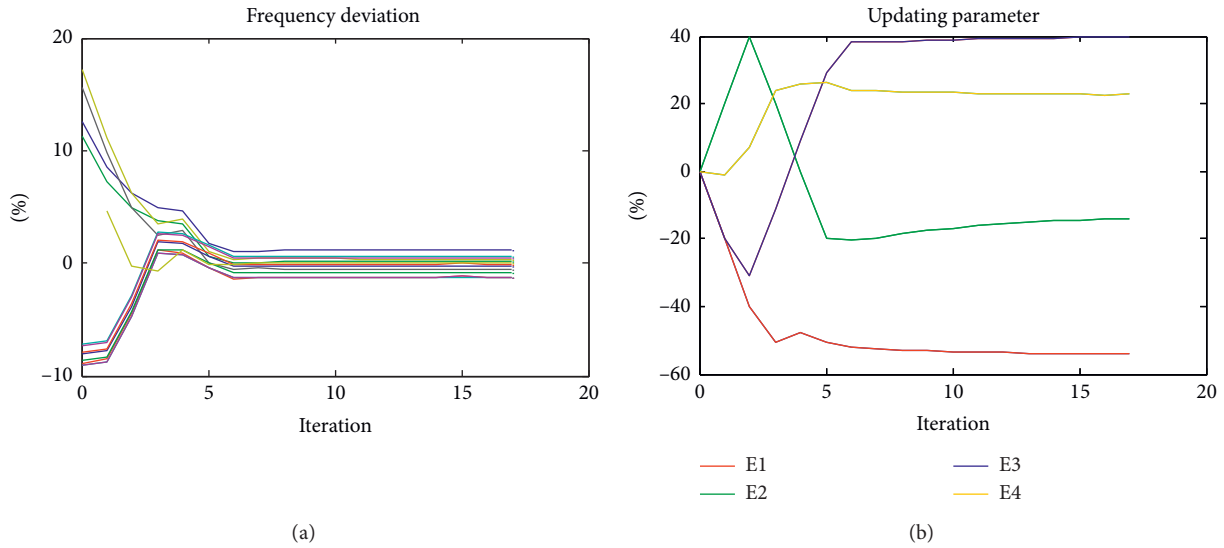

Figure 25: Updating process using RTM and frequency data.

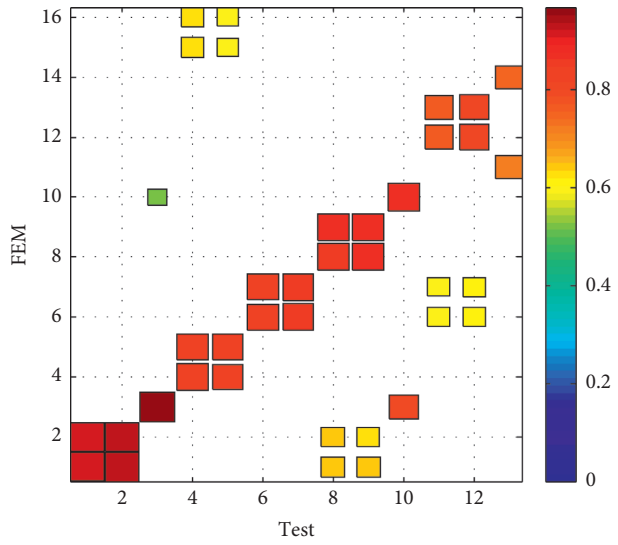

Figure 26: Correlation analysis using RTMs between the test and the FE model after updating.

Table 9: Frequency deviation and RTM correlation values before and after model updating.

Test		FEM				Frequency deviation (%)		MAC (%)		RTMAC (%)	
		Initial FEM		Updated FEM							
Mode	Natural frequency	Mode	Natural frequency	Mode	Natural frequency	Initial	Updated	Initial	Updated	Initial	Updated
1	634.67	2	714.66	1	642.48	12.60	1.23	53.57	78.68	91.74	92.02
2	642.16	1	714.40	2	643.48	11.25	0.21	49.73	76.46	91.74	93.50
3	864.28	3	787.41	3	853.85	−8.89	−1.21	98.78	98.79	96.81	96.91
4	1617.86	4	1471.24	4	1598.17	−9.06	−1.22	68.15	68.48	83.74	84.12
5	1620.11	5	1473.49	5	1600.44	−9.05	−1.21	57.89	58.65	81.92	82.56
6	1928.52	9	2258.94	6	1935.65	17.13	0.37	78.73	55.17	84.68	83.66
7	1953.65	8	2258.86	7	1943.67	15.62	−0.51	79.88	61.24	86.85	85.78
8	2452.27	7	2253.15	9	2445.97	−8.12	−0.26	93.83	94.30	86.02	86.40
9	2464.95	6	2251.54	8	2444.09	−8.66	−0.85	93.00	92.86	86.99	87.43
10	3019.31	10	2780.27	10	3017.49	−7.92	−0.06	89.98	89.94	87.02	86.99
11	3521.61	12	3266.38	13	3544.50	−7.25	0.65	77.84	76.61	75.46	76.85
12	3526.16	11	3265.81	12	3543.99	−7.38	0.51	80.84	82.86	79.19	80.61
13	3912.75	16	4325.20	14	3912.86	10.54	0.00	16.45	80.70	72.05	74.44

Table 10: Comparison of initial and updated parameters.

Updating parameter	Initial (GPa)	Modified (GPa)	Change (%)
E1	184	84.4	−54.13
E2	184	158	−14.13
E3	184	257	39.67
E4	184	226	22.83

hence these may be considered as the discretization errors of the two groups that is equivalent to a change in the elastic modulus. Above all, the example of the cover structure demonstrates the feasibility of using RTMs in correlation analysis and model updating.

5. Conclusion

The implementation of radial Tchebichef moment descriptors can effectively extract features of vibration mode shapes of symmetric structures and is able to compress the full-field modal vibration data. The most important information of the mode shapes is retained in the form of radial Tchebichef moment descriptors. The rotational angle of the double/close modes of symmetric structures can be identified as well with RTMs. The simulation analysis to deal with the images of mode shapes from a disk structure shows that mode shape reconstruction using the radial Tchebichef moments has more advantage than that using the Zernike moments. With the increase of the moment order, reconstruction using RTMs shows the better quality and higher stability, compared to the reconstruction using Zernike moments. In addition, the proposed modal correlation coefficient of RTM amplitude can overcome the main disadvantage of using the modal assurance criterion (MAC), which has difficulty in identifying double or close modes of symmetric structures. The model updating of axisymmetric structures based on RTM descriptors can speed up the convergence of updating parameters without dealing with large amounts of mode shape data. The RTM descriptors used in correlation analysis and model updating are demonstrated with a cover of an aeroengine test rig. A modal test was performed, and an FE model was built. The results showed that the frequency deviation between the test and the FE model reduced from 17.13% to 1.23% after model updating for the first 13 modes. It demonstrates the effectiveness and efficiency of the proposed method.

Data Availability

The data used to support the findings of this study are available from the corresponding author upon request.

Conflicts of Interest

The authors declare that there are no conflicts of interest.

Acknowledgments

The authors gratefully appreciate the financial support for this work provided by the National Natural Science Foundation of China and National Safety Academic Foundation of China (Nos. 12072146 and U1730129). The supports from Jiangsu Province Key Laboratory of Aerospace Power System, the Key Laboratory of Aero-Engine Thermal Environment and Structure, and Ministry of Industry and Information Technology are also gratefully acknowledged.

References

[1] J. E. Mottershead, M. Link, and M. I. Friswell, "The sensitivity method in finite element model updating: a tutorial," *Mechanical Systems and Signal Processing*, vol. 25, no. 7, pp. 2275–2296, 2011.

[2] J. M. W. Brownjohn and P.-Q. Xia, "Dynamic assessment of curved cable-stayed bridge by model updating," *Journal of Structural Engineering*, vol. 126, no. 2, pp. 252–260, 2000.

[3] R. J. Allemang and D. L. Brown, "A correlation coefficient for modal vector analysis[C]//Proceedings of the 1st International Modal Analysis Conference," *SEM, Orlando*, vol. 1, pp. 110–116, 1982.

[4] C. W. Schwingshackl, L. Massei, C. Zang, and D. J. Ewins, "A constant scanning LDV technique for cylindrical structures: simulation and measurement," *Mechanical Systems and Signal Processing*, vol. 24, no. 2, pp. 394–405, 2010.

[5] A. B. Stanbridge, M. Martarelli, and D. J. Ewins, "Measuring area vibration mode shapes with a continuous-scan LDV," *Measurement*, vol. 35, no. 2, pp. 181–189, 2004.

[6] Á. J. Molina-Viedma, E. López-Alba, L. Felipe-Sesé, and F. A. Díaz, "Full-field modal analysis during base motion excitation using high-speed 3D digital image correlation," *Measurement Science and Technology*, vol. 28, no. 10, p. 105402, 2017.

[7] M. K. Hu, "Visual pattern recognition by moment invariants," *Information Theory, IRE Transactions on*, vol. 8, no. 2, pp. 179–187, 1962.

[8] S. S. Reddi, "Radial and angular moment invariants for image identification," *IEEE Transactions on Pattern Analysis and Machine Intelligence*, vol. PAMI-3, no. 2, pp. 240–242, 1981.

[9] B. Bamieh and R. De Figueiredo, "A general moment-invariants/attributed-graph method for three-dimensional object recognition from a single image," *IEEE Journal on Robotics and Automation*, vol. 2, no. 1, pp. 31–41, 1986.

[10] Y. S. Abu-Mostafa and D. Psaltis, "Recognitive aspects of moment invariants," *IEEE Transactions on Pattern Analysis and Machine Intelligence*, vol. PAMI-6, no. 6, pp. 698–706, 1984.

[11] M. R. Teague, "Image analysis via the general theory of moments∗," *Journal of the Optical Society of America*, vol. 70, no. 8, pp. 920–930, 1980.

[12] C.-H. Teh and R. T. Chin, "On image analysis by the methods of moments," *IEEE Transactions on Pattern Analysis and Machine Intelligence*, vol. 10, no. 4, pp. 496–513, 1988.

[13] H. Hse and A. R. Newton, "Sketched symbol recognition using Zernike moments," in *Proceedings of The 17th International Conference on Pattern Recognition, 2004. ICPR 2004*, vol. 1, pp. 367–370, IEEE, Cambridge, UK, August 2004.

[14] H. S. Kim and H. K. Lee, "Invariant image watermark using Zernike moments," *IEEE Transactions on Circuits and Systems for Video Technology*, vol. 13, no. 8, pp. 766–775, 2003.

[15] Y. Liu and C. Zang, "Mode shape description of an aeroengine casing structure using Zernike moment descriptors," *Journal of Aerospace Power*, vol. 26, no. 4, 2011.

[16] R. Mukundan, S. H. Ong, and P. A. Lee, "Image analysis by Tchebichef moments," *IEEE Transactions on Image Processing*, vol. 10, no. 9, pp. 1357–1364, 2001.
[17] P. T. Yap, R. Paramesran, and S. H. Ong, "Image analysis by Krawtchouk moments," *IEEE Transactions on Image Processing*, vol. 12, no. 11, pp. 1367–1377, 2003.
[18] H. Zhu, H. Shu, J. Liang, L. Luo, and J.-L. Coatrieux, "Image analysis by discrete orthogonal Racah moments," *Signal Processing*, vol. 87, no. 4, pp. 687–708, 2007.
[19] H. Zhu, H. Shu, J. Zhou, L. Luo, and J. L. Coatrieux, "Image analysis by discrete orthogonal dual Hahn moments," *Pattern Recognition Letters*, vol. 28, no. 13, pp. 1688–1704, 2007.
[20] R. Mukundan, "Radial Tchebichef invariants for pattern recognition," in *Proceedings of the TENCON 2005 IEEE Region 10*, pp. 1–6, IEEE, Melbourne, Australia, November 2005.
[21] W. Wang, J. E. Mottershead, and C. Mares, "Mode-shape recognition and finite element model updating using the Zernike moment descriptor," *Mechanical Systems and Signal Processing*, vol. 23, no. 7, pp. 2088–2112, 2009.
[22] W. Wang, J. E. Mottershead, A. Ihle, T. Siebert, and H. Reinhard Schubach, "Finite element model updating from full-field vibration measurement using digital image correlation," *Journal of Sound and Vibration*, vol. 330, no. 8, pp. 1599–1620, 2011.
[23] Y. Liu and C. Zang, "Mode shape description of a symmetrical structure using Zernike moment descriptors," *Journal of Vibration Engineering*, vol. 24, no. 4, pp. 369–375, 2011.
[24] C. Zang and Y. Liu, "Mode shape description and model validation of axisymmetric structure," *Journal of Nanjing University of Aeronautics and Astronautics*, vol. 44, no. 5, pp. 725–733, 2012.
[25] R. Mukundan, "A comparative analysis of radial-Tchebichef moments and zernike moments," in *Proceedings of the British Machine Vision Conference BMVC*, pp. 1–7, London, UK, September 2009.